Journal of Solid State Chemistry **154,** 33–38 (2000)
doi:10.1006/jssc.2000.8807, available online at http://www.idealibrary.com on IDEAL®

Electrical and Thermal Properties of $B_{12}P_2$ Wafers

Y. Kumashiro, T. Yokoyama, K. Sato, and Y. Ando

Faculty of Engineering, Yokohama National University, 79-5 Tokiwadai, Hodogaya-ku, Yokohama, 240-8501, Japan

and

S. Nagatani and K. Kajiyama

MAC Science Company Ltd.1-5-1 Shinyokohama, Kohoku-ku, Yokohama, 222-0033, Japan

Received September 9, 1999; in revised form March 16, 2000; accepted March 31, 2000

Electrical and thermal properties of semiconducting $B_{12}P_2$ wafers designed as $B_{12}(Si_2)_x(P_2)_{1-x}$ were measured up to high temperature. The wafers were grown at 1100°C by thermal decomposition of a B_2H_6–PH_3–H_2 gas mixture at 1100°C on Si(100) and Si(111) substrates in long-term experiments. The electrical conductivity obeyed band conduction. Thermoelectric power showed high values of 800–1000 μV/K at 400–800 K. Measurement of the specific heat capacity by differential scanning calorimetry (DSC) yielded Debye temperatures of 1200–1300 K and Grüneisen parameters of 0.8–0.9. Thermal diffusivity was measured with the use of ring-flash light in the laser flash method. The weak temperature dependence of thermal conductivity reflects phonon scattering by Si impurities rather than by grain boundaries. Low electrical conductivity produces lower thermoelectric figures-of-merit than BP wafers despite the high thermoelectric power. © 2000 Academic Press

INTRODUCTION

There are two refractory boron phosphides: boron monophosphide (BP) with a zinc-blende structure and boron subphosphide ($B_{12}P_2$) with a rhombohedral structure. The boron monophosphide is well known as a refractory semiconductors (1,2), but the rhombohedral boron phosphide is a wide-gap (3.3 eV) semiconductor (3).

The structure of rhombohedral boron phosphide is similar to that of α-boron, but has chains of two phosphorus atoms lying within the rhombohedron, connected to six B_{12} icosahedra by two-center bonds (4).

We have succeeded in preparing semiconducting $B_{12}P_2$ wafers doped with Si atoms in a chemical vapor deposition (CVD) process at a high temperature of 1100°C (5). The present paper describes electrical properties, i.e., high-temperature electrical conductivity and Seebeck effect, and high-temperature thermal characteristics, i.e., heat capacity by differential scanning calorimetry (DSC) and thermal diffusivity by ring-flash light method, of semiconducting $B_{12}P_2$ wafers to clarify their intrinsic thermophysical properties.

EXPERIMENTAL

The horizontal CVD apparatus was the same as that described in our previous report on BP (6). The reaction chamber was made of fused quartz with the upper part cooled by running water. Two slopes (6) were placed in front of and to the rear of the SiC-coated graphite susceptor, which removed the vortex flow at the susceptor, giving a more uniform temperature at the substrate. The susceptor was heated externally by an RF generator, and the substrate temperature of 1100°C was measured with an optical pyrometer. Boron subphosphide ($B_{12}P_2$) wafers ($20 \times 10\,mm^2$, 0.1-mm thickness) were grown on Si(100) and Si(111) planes under the optimum conditions (7) of flow rates of B_2H_6(1% in H_2) = $30\,cm^3$/min, $PH_3 = 30\,cm^3$/min for 16 hr and were obtained by dissolving the silicon substrate in concentrated HF + concd HNO_3 (1 : 5) solution. Electrical properties at room temperature were measured by the van der Pauw method. Electrical conductivity of the wafers was measured by a two-probe method between room temperature and 800°C under an argon atmosphere. Thermoelectric voltage between hot and cold junctions was measured under a constant temperature gradient of 2–3°C (2). The specific heat capacity was measured on small wafers by DSC in the temperature range 60–500°C. Thermal diffusivity of wafers was measured by the laser-flash method using a ring flash light (8). We consider a homogeneous circular plate in a cylindrical coordinate systems. Laser light irradiates the specimen in the form of a ring with an inner radius and outer radius. The temperature $T(x, r, t)$ at radius r and distance x from the central axis of the disk can be derived from general solutions of the heat conduction equation for

0022-4596/00 $35.00

a cylindrical sample. For details see (8). Thin graphite films with a thickness of $\sim 5\,\mu m$ were sprayed on both faces of the wafer with a dry graphite film lubricant (dgl 123 produced by Japan Ship Machine Tool Co. Limited). Thermal conductivity was calculated from the product of the thermal diffusivity, heat capacity, and density.

RESULTS

A. Characterization of the Wafers

The lattice mismatch between $B_{12}P_2$ and Si(100) and Si(111) planes is large, depending on the orientation (7). Furthermore the existence ratios and distribution of various $B_{12}P_2(11\bar{2}0)$, $(10\bar{1}1)$, $(02\bar{2}1)$, and $(10\bar{1}0)$ planes change along the growth direction and are influenced by the location on the substrate, whether upstream or downstream regions of the substrate (7). These facts would produce the polycrystalline wafer for a long-time growth experiment [5]. A SEM image of the $B_{12}P_2$ wafer shows a grain size of $\sim 2\,\mu m$ (Fig. 1).

The content of Si atoms in $B_{12}P_2$ film by SIMS indicates that 10^{22} Si atoms/cm^3 at the $B_{12}P_2$/Si interface decreases to 10^{21} Si atoms/cm^3 at the first 3 μm adjacent to the Si substrate and to 10^{19}–10^{20} Si atoms/cm^3 in the film. The concentration of Si in the wafer would average 10^{20}–10^{21} atoms/cm^3. Si contents are detected by IR spectra (5,9). The absorption coefficient in the edge tail (10) is detected due to the Si content. The X-ray diffraction pattern of the present $B_{12}P_2$ wafer indicates precipitation of Si shown in Fig. 2.

The $B_{12}P_2$ doped with Si in the present study has unit cell parameters of $a = 6.00$ Å, $c = 12.0$ Å (10), indicating a c axis elongated with respect to pure $B_{12}P_2$, i.e., $a = 6.000$ Å, $c = 11.857$ Å (11). This change agrees with the tendency toward the unit parameters of $B_{2.89}Si$ ($a = 6.319$ Å, $c = 12.713$ Å) (11) and the modifications in boron-rich boron carbide induced by doping with silicon (12,13). The Si atoms form Si_2 chains in these unit cells of $B_{12}P_2$ designated

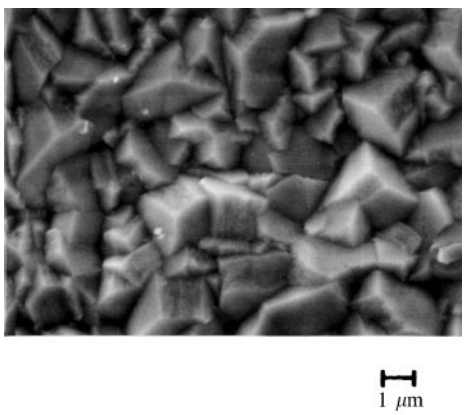

FIG. 1. SEM image of the $B_{12}P_2$ wafer.

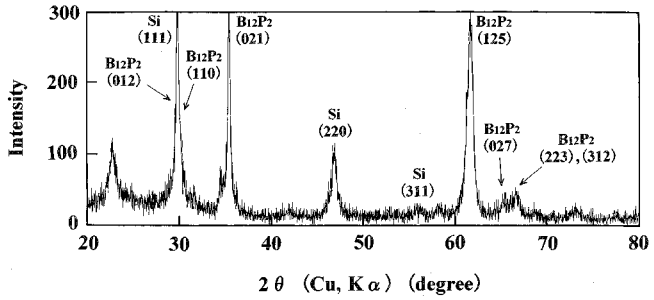

FIG. 2. X-Ray diffraction pattern of $B_{12}P_2$ wafer.

$B_{12}(Si_2)_x(P_2)_{1-x}$ (10), which would be supported by the change in unit cell parameter depending on the P content of undoped $B_{12}P_2$ (14).

The electrical properties of these $B_{12}P_2$ wafers doped with Si are listed in Table 1. They are all *p*-type semiconductors. The resistivity of the wafers is lower than the cited value (15) by 10^4–10^5 so that the autodoped Si from the Si substrate would affect the electrical properties.

B. Thermal and Electrical Properties up to High Temperatures

The temperature dependence of electrical conductivity (σ) is shown in Fig. 3, which includes the results for polycrystalline $B_{11.6}P_2$ of Greiuer and Guotwski (16). The electrical conductivity of $B_{12}P_2$ obeys band conduction with an activation energy of 0.85 eV, which would correspond to that of the intrinsic region.

The temperature dependence of thermoelectric power is shown in Fig. 4. The thermoelectric power values of $B_{12}P_2$ wafers are high, 800–1000 μV/K at 400–800 K. High thermoelectric power is consistent with low carrier concentration (2) in the specimen (Table 1).

Figure 5 shows the specific heat capacity of semiconducting $B_{12}P_2$ wafers. The specific heat capacity increases with increasing temperature, but no appreciable difference was observed between samples grown on Si(100) and Si(111) planes. The temperature dependence of the thermal diffusivity is shown in Fig. 6.

TABLE 1
Electrical Properties of $B_{12}P_2$ Wafer

Substrate	Conduction type	Electrical resistivity (Ω·cm)	Carrier concentration (cm^{-3})	Mobility (cm^2·V^{-1}·s^{-1})
Si (100)	*p*	1.4×10^5	1.4×10^{12}	31.7
Si (111)	*p*	6.2×10^4	9.3×10^{13}	10.8

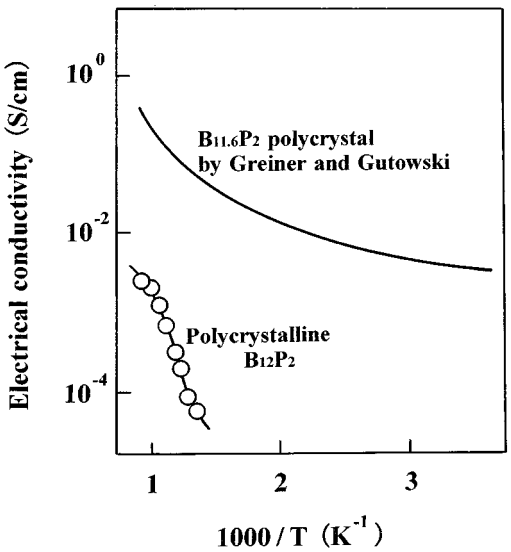

FIG. 3. Temperature dependencies of electrical conductivities of semiconducting $B_{12}P_2$ polycrystals. The result for $B_{11.6}P_2$ (16) is also shown.

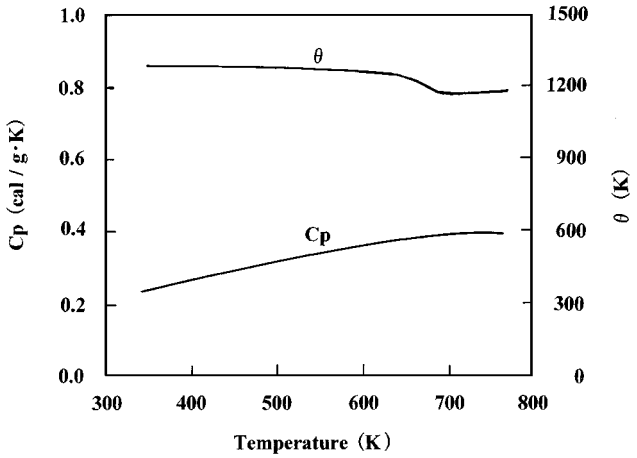

FIG. 5. Temperature dependencies of specific heat capacity (C_p) and Debye temperature (θ) of semiconducting $B_{12}P_2$ polycrystal.

The temperature dependence of thermal conductivity, calculated as the product of thermal diffusivity (Fig. 6), specific heat capacity (Fig. 5), and density (15), is shown in Fig. 7. The results are compared with those for boron carbide ($B_{1-x}C_{1-x}$) (17), the structure of which is a modification of α-B structure, being similar to the $B_{12}P_2$ structure. The configuration of the specimen $x = 0.2$, i.e., B_4C, in the intericosahedral chains is carbon–boron–carbon (CBC) while that of $x = 0.1$, i.e., B_9C, is CBB. The temperature dependence of the thermal diffusivity for $B_{1-x}C_x$ changes from that typical of crystalline solids (falling with increasing temperature) at high carbon concentrations of $x > 0.18$ to that characteristic of a glass (nearly independent of temperature) at low carbon concentrations of $x < 0.17$ (17).

DISCUSSION

If $B_{12}P_2$ has no impurity, the concentration of phosphorus atoms is 1.24×10^{21} atoms/cm^3, which produces $x = 0.07$ in $B_{12}(P_2)_{1-x}(Si_2)_x$. However, the concentrations of the ionized silicon acceptor measured by the electrical properties (Table 1) are much smaller than normal silicon contents by about 10^8–10^9, indicating that most silicon atoms would remain as neutral impurity and Si precipitation (Fig. 2).

In comparing our data in Fig. 3 with those of Greiner and Guotwski (16), their specimens contain < 0.03 wt% Si, < 0.01 wt% Cu, and magnesium, so their sample is less

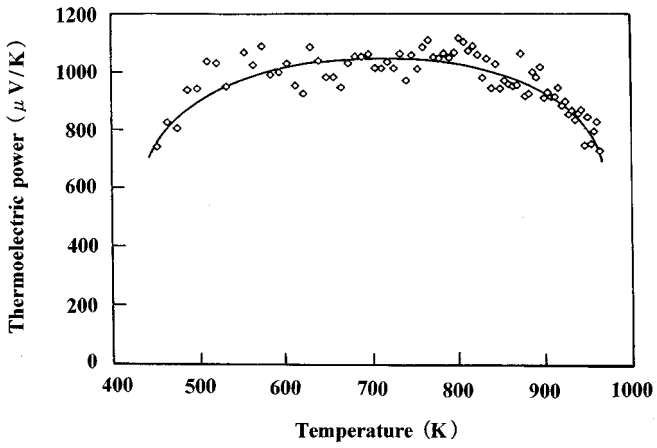

FIG. 4. Temperature dependence of thermoelectric power of semiconducting $B_{12}P_2$ polycrystal.

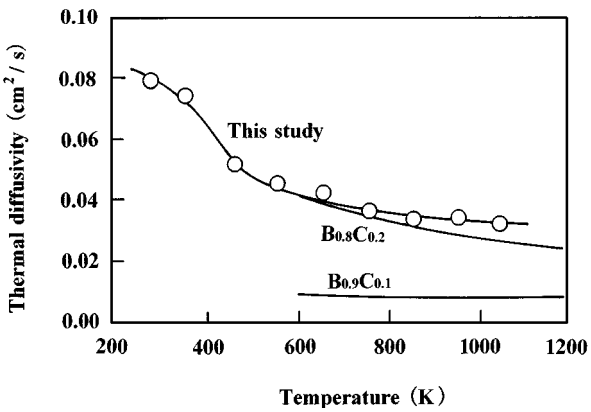

FIG. 6. Temperature dependence of the thermal diffusivity of semiconducting $B_{12}P_2$ polycrystal. The results for $B_{1-x}C_x$ (17) are also shown.

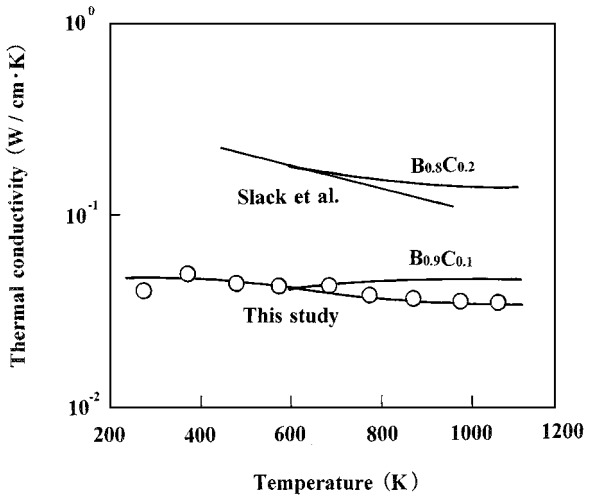

FIG. 7. Temperature dependencies of the thermal conductivity of $B_{12}P_2$. The results of Slack *et al.* (22) and $B_{1-x}C_x$ (17) are also shown.

pure than ours. Their specimens are significantly higher in the intrinsic-like conductivity range. The determined activation energy of 0.85 eV would be correlated with a gap of 1.7 eV in rather good agreement with the optically determined value (10). This would suggest intrinsic and not extrinsic behavior.

The thermoelectric power increases with increase in temperature up to 400 K (Fig. 4). It tends to saturate and then decreases with a rise in temperature. This result cannot be explained by assuming only one kind of carrier. At higher temperatures the wafer approaches the intrinsic range, and both holes and electrons contribute to the thermoelectric power, with cancelling contributions to the measured voltage. The same behavior is observed in *p*-type BP wafers (18). Furthermore Pistoulet *et al.* (19) explained the electrical properties of B–Si compounds of composition close to that of $B_{14}Si$ by using a model based on medium-range disorder. The spatial fluctuations of composition produce spatial fluctuation in the potential, where the thermoelectric power-versus-temperature curve has a maximum value. From these experimental results the temperature dependence of thermoelectric power in our specimen would be reasonable.

The specific heat capacity gives the value of the Debye temperature θ. The value of θ is obtained from specific heat at constant volume C_V, which is deduced with the usual thermodynamic formula

$$C_V = C_p - (\beta^2 V)/KT, \qquad [1]$$

where β is the volume expansivity ($\beta = 3\alpha$, where α is linear expansivity), K the isothermal compressibility, and V the molar volume. There are no data on α and K for $B_{12}P_2$ so the data for boron carbide (20) were used with the values of $V = 69.44\ \text{cm}^3$ and the published data for α (20). K was calculated by Young modulus E (20) and Poission ratio (20). C_p (Fig. 5) is converted to C_V. Then θ is calculated with the formula

$$C_V/42R = (3/x)\int_0^{x_0} [x^4 e^x/(e^x - 1)^2]\, dx \quad \text{with } x = \theta/T, \qquad [2]$$

where R is the gas constant of 1.987 cal/mol·K. The values of the right-hand term in Eq. [2] have been tabulated (21). The temperature dependence of θ is shown in Fig. 5. Slack *et al.* (22) estimated θ by using a scaling law devised by Steigmeir (23) to obtain $\theta = 1160$ K at room temperature. Our data are higher than theirs and near to β-B of 1300 K, which would be due to the uncertainty of the parameter used. It remains almost constant up to 650 K, where it begins to fall (Fig. 5). This decrease is due to the excess specific heat which may be associated with the anharmonicity of the lattice. The Debye temperature and its temperature dependence for the crystal we examined should be typical of the results for boron phosphide: a high Debye temperature reflects the low atomic mass and strong interatomic bonding in boron phosphide.

The Grüneisen parameter γ was calculated to see the anharmonic character of $B_{12}P_2$. For this purpose Eq. [1] is rewritten as

$$C_p = C_V(1 + \gamma\beta T), \qquad [3]$$

$$\gamma = \beta V/KC_V. \qquad [4]$$

Figure 8 shows γ as a function of reduced temperature T/θ. γ values have almost the same limiting value of about 0.8 at $T \sim \theta$ and decrease with decreasing temperature. Large γ means high anharmonicity and small variations would be its low ionicity.

Vibrational energy is transported with a charge carrier. The present $B_{12}P_2$ wafer has a low carrier concentration

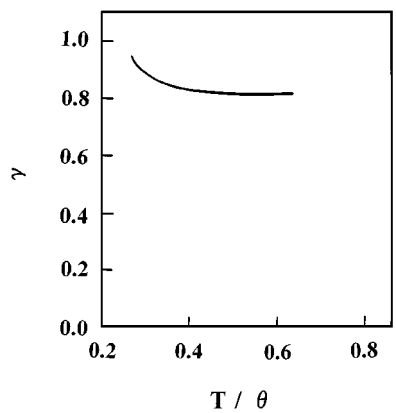

FIG. 8. Grüneisen parameter of semiconducting $B_{12}P_2$ polycrystal as a function of the reduced temperature.

(Table 1) so conduction of heat by a mobile carrier may be neglected. But transported energy increases with temperature. The electronic contribution to the thermal conductivity is a product of transported energy, electronic diffusion constant, and the rate of change of the carrier density with temperature, which yield very small increases with temperature (24). The electronic contribution to the thermal conductivity relative to the lattice contribution is neglected.

The thermal transport in B_4C is crystal-like while that in B_9C is amorphous glass (Fig. 7) (25). In the present $B_{12}P_{2x}(Si_2)_{1-x}$ the thermal conductivity would be characteristic of a crystal in the temperature dependence inductive of thermal tranport via phonons. Low magnitude and weak temperature dependence of the thermal conductivity would be due to defect scattering, indicative of some disorder that scatters the phonon in the lattice in comparison with more perfect crystalline $B_{12}P_2$ (22) in Fig. 7. Some disorder would be considered as Si precipitate in the specimen confirmed by X-ray diffraction (Fig. 2) and absorption spectra (10). To see any effects on thermal conductivity due to grain boundaries, the lattice thermal conductivity can be discussed in terms of a phonon gas having a particular specific heat (C) and mean free path ($\bar{l}$) (24, 25).

Thermal conductivity is given by

$$\kappa = C\rho v\bar{l}/3, \qquad [5]$$

where C is the specific heat per unit mass, ρ is the mass density, and, v the average sound velocity of phonon, which does not change largely, so thermal conductivity is determined mainly by heat capacity and mean free path of phonon. Using the specific heat and thermal conductivity data and sound velocity of B_4C (25), we estimate an average mean free path of 1.1×10^{-3} μm at 300 K being much smaller than ~2 μm for the grain size of the wafer (Fig. 1). Slack *et al.* (22) measured the thermal conductivity of isomorphous compounds $B_{12}As_2$, $B_{12}P_2$, and $B_{12}C_3$ below some temperature so the mean free path of these phonons is about 2×10^{-2} μm for temperatures near the Debye temperature decreases, i.e., 1 μm at room temperature. The phonons are scattered by grain boundarries at low temperature and by impurities at high temperature (24). Then the thermal conductivity in the present wafer would not be affected by scattering from grain boundary.

The thermoelectric figure-of-merit Z ($=\alpha^2\sigma/\kappa$) is shown in Fig. 9. The Z value increases with increasing temperature, reaching $\sim3\times10^{-8}$/K, but is an BP by two orders of magnitude. The thermal conductivity of $B_{12}P_2$ wafer is almost same as that of BP polycrystal, but low electrical conductivity produces lower Z, despite high thermoelectric power (Fig. 4). Their specimens are significantly higher in the intrinsic-like conductivity range. The electrical conductivity of our wafer would increase by optimum substitution of Si in $B_{12}P_2$. In this case thermoelectric power would be reduced but the Z value would be expected to increase.

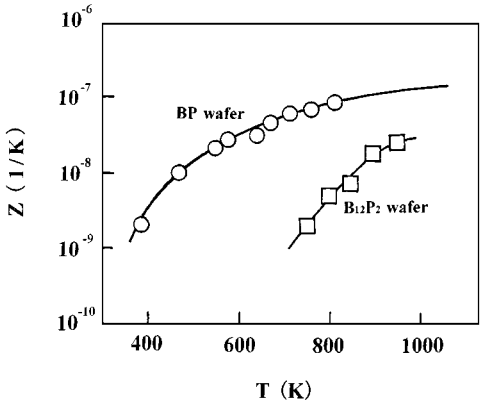

FIG. 9. Thermoelectric figure-of-merit for boron monophosphide (BP) and boron subphosphide ($B_{12}P_2$) wafers as a function of temperature.

CONCLUSION

We have measured electrical and thermal properties of semiconducting $B_{12}P_2$ wafers by autodoped Si atoms. The resistivity of $B_{12}P_2$ wafers is lower than the cited value by 10^4–10^5. The Si atoms contributing to semiconduction are far smaller than normal Si contents. The heat capacity induces a high Debye temperature of 1200–1300 K and Grüneisen parameter of 0.8–0.9. Thermal conductivity calculated by the products of heat capacity, thermal diffusivity, and density shows weak temperature dependence over the entire temperature range by phonon scattering by Si impurities. The low electrical conductivity of the present $B_{12}P_2$ wafer produces lower thermoelectric figures-of-merit than BP by about two orders of magnitude, despite high thermoelectric power. Then optimum doping of Si would be necessary to promote electrical conductivity.

ACKNOWLEDGMENTS

This work was supported by a Grant-in-Aid for Science Research (06805061) from the Ministry of Education and Nippon Sheet Glass Foundation for Materials Science and Engineering.

REFERENCES

1. Y. Kumashiro, *J. Mater. Res.* **5,** 2933 (1989).
2. Y. Kumashiro, T. Yokoyama, A. Sato, and Y. Ando, *J. Solid State Chem.* **133,** 314 (1997).
3. G. E. Slack, T. F. McNelly, and E. A. Taft, *J. Phys. Solids* **44,** 1009 (1983).
4. D. Emin, *Phys. Today* **40,** 55 (1987).
5. Y. Kumashiro, H. Yoshizawa, and K. Shirai, *JJAP Ser.* **10,** 166 (1994).

6. Y. Kumashiro, Y. Okada, and H. Okumura, *J. Cryst. Growth* **132,** 611 (1993).
7. Y. Kumashiro, H. Yoshizawa, and T. Yokoyama, *J. Solid State Chem.* **133** (1997).
8. Y. Kumashiro, T. Mitsuhashi, S. Okaya, F. Muta, T. Koshiro, M. Hirabayashi, and Y. Okaya, *High Temp.-High Press.* **21,** 105 (1989).
9. K. Shirai, S. Gonda, and Y. Kumashiro, *JJAP Ser.* **10,** 102 (1993).
10. H. Werheit, U. Kuhlman, K. Shirai, and Y. Kumashiro, *J. Alloys Compd.* **233,** 121 (1996).
11. T. Lundström, *AIP Conf. Proc.* **231,** 186 (1990).
12. H. Werheit, U. Kuhlman, M. Laux, and R. Telle, *J. Alloys Compd.* **209,** 181 (1994).
13. H. Werheit, U. Kuhlman, M. Laux, and R. Telle, *JJAP Ser.* **10,** 86 (1994).
14. E. Amberger and P. A. Rauh, *Acta Crystallogr. Sect. B* **30,** 2549 (1974).
15. J. L. Peret, *J. Am. Ceram. Soc.* **47,** 44 (1964).
16. E. S. Greiuer and J. A. Guotwski, *J. Appl. Phys.* **30,** 18421 (1959).
17. C. Wood, D. Emin, and P. E. Gray, *Phys. Rev. B* **21,** 6811 (1985).
18. S. Yugo and T. Kimura, *Phys. Status Solidi A* **59,** 363 (1980).
19. B. Pistoulet, J. L. Robert, J. M. Dusseau, F. Roche, P. Girard, and L. Ensuque, *J. Less-Common Met.* **67,** 131 (1979).
20. R. A. Murgatroyd and B. T. Kelly, *At. Energ. Rev.* **15,** 3 (1979).
21. E. S. R. Gopal, "Specific Heats at Low Temperature," p. 221, Plenum, New York, 1966.
22. G. A. Slack, D. W. Oliver, and F. H. Horn, *Phys. Rev. B* **4,** 1714 (1971).
23. E. F. Steigmer, *Appl. Phys. Lett.* **3,** 6 (1963).
24. D. G. Cahil, H. F. Fischer, S. K. Watson, R. D. Pohl, and G. A. Slack, *Phys. Rev. B* **40,** 3254 (1989).
25. P. A. Medwick, H. E. Fischer, and R. O. Pohl, *J. Alloys Compd.* **203,** 67 (1994).